Available online at www.sciencedirect.com
SCIENCE DIRECT®
Thermochimica Acta 403 (2003) 89–103
thermochimica acta
www.elsevier.com/locate/tca

Advanced two-channel ac calorimeter for simultaneous measurements of complex heat capacity and complex thermal conductivity

A.A. Minakov [a,*], S.A. Adamovsky [b], C. Schick [b]

[a] *Natural Science Center of General Physics Institute, Vavilov Street 38, 199911 Moscow, Russia*
[b] *Department of Physics, University of Rostock, Universitatsplatz 3, 18051 Rostock, Germany*

Received 6 October 2002; received in revised form 5 February 2003; accepted 6 February 2003

Abstract

The advanced construction of a two-channel ac calorimeter for simultaneous measurements of frequency-dependent complex heat capacity $\boldsymbol{C}(\omega)$ and complex thermal conductivity $\boldsymbol{\lambda}(\omega)$ is presented. In the new calorimeter, the number of interfaces with thermal-wave reflections was reduced. Thus, the new construction can be easily calibrated with higher precision and is simpler in handling than the previous one. The new construction allows to measure thermal conductivity in steady-state mode, as well as frequency-dependent complex thermal properties in ac mode, in the same measuring cell. The capabilities of this technique were demonstrated, being applied for simultaneous measurements of complex effusivity, diffusivity, heat capacity, and thermal conductivity of glycerol in the glass transition region. The so-called ac and dc thermal conductivities of glycerol were measured as a function of temperature. It was shown that the double-channel ac calorimetry is a technique, which can be used for reliable distinguishing of relaxation processes related to relaxing thermal conductivity or relaxing heat capacity.

In the region apart from phase transitions, the calorimeter provides the unique possibility of simultaneous measurements of the thermal contact properties together with the sample's thermal parameters. The improvement of the accuracy gave us the possibility to observe the thermal contact resistance, leading to a step of 1 and 5% in the temperature-modulation amplitude at the cell/sample interface in the case of liquid samples such as Apiezon™-H grease and glycerol, respectively. A step of 25% was observed in the case of a dry thermal contact between the cell and an ethylene-1-octene copolymer sample. Thus, the thermal contact resistance must be taken into account in the temperature-modulated calorimetry, especially in the case of a dry cell/sample contact.

Keywords: Complex heat capacity; Complex thermal conductivity; Temperature-modulation calorimetry; Glass transition; Thermal contact resistance

1. Introduction

Frequency-dependent complex heat capacity, $\boldsymbol{C}(\omega)$, provides important information on relaxation phenomena at glass, melting and crystallization transitions. In general, the thermal properties of a system, which are measured at a temperature-modulation frequency ω, can be complex and frequency-dependent near a phase transition, where slowly relaxing processes occur.

The first measurement of the complex heat capacity of amorphous selenium was reported by Gobrecht et al. [1]. Then, the so-called 3-ω method was applied

* Corresponding author. Tel.: +7-95-132-82-68; fax: +1-95-135-82-81.
E-mail address: minakov@nsc.gpi.ru (A.A. Minakov).

0040-6031/03/$ – see front matter © 2003 Elsevier Science B.V. All rights reserved.
doi:10.1016/S0040-6031(03)00090-X

for the measurements of the frequency-dependent complex heat capacity near glass transition in glycerol and propylene glycol by Birge and Nagel [2] and Birge [3]. Next, a photoacoustic (PA) method was applied for analogous measurements in polymers [4]. Strictly speaking, the thermal effusivity $\boldsymbol{e}(\omega) = (\boldsymbol{c} \cdot \boldsymbol{\lambda})^{1/2}$ was measured by PA and 3-ω techniques, where $\boldsymbol{c}$ and $\boldsymbol{\lambda}$ are specific heat capacity and thermal conductivity, respectively. The frequency dependence $\boldsymbol{c}(\omega)$ was extracted from the thermal effusivity $\boldsymbol{e}(\omega)$ under the assumption that the thermal conductivity is frequency independent. This assumption may be not always correct. Varying the width of the heater, one can choose the proper regime to measure by 3-ω method thermal conductivity or specific heat capacity [5,6]. Another combination of $\boldsymbol{c}$ and $\boldsymbol{\lambda}$, the thermal diffusivity $\boldsymbol{\alpha}(\omega) = \boldsymbol{\lambda}/\boldsymbol{c}$, can be obtained from the measurements of phase and amplitude of a thermal wave transmitted through a plate-like sample [7,8]. The method was named thermal wave analysis (TWA). A similar technique, named thermal wave transmission spectroscopy (TWTS) [9,10], was developed on the basis of an ac calorimeter [11]. Complex heat capacity can be measured directly by means of temperature-modulated differential scanning calorimetry (TMDSC) [1,12–15], but this method is limited by an infra-low frequency range, ca. 1–100 mHz.

In all these techniques, an oscillating heat flow $P_0 \cos(\omega t)$ is supplied to one side of a plate-like sample and the temperature oscillations $T_0 \sin(\omega t + \varphi)$ are measured on the same side, as in TMDSC, PA and 3-ω method, or on the other side, which is opposite to the heat flow, as in TWA or TWTS. The measured parameters, P_0, T_0, and φ, provide information on real (Re) and imaginary (Im) parts of an appropriate sample's thermal parameter. Thus the complex thermal effusivity $\boldsymbol{e}(\omega)$ is determined by PA and 3-ω method. In this case, the sample is thick enough to be assumed as semi-infinite. The complex diffusivity $\boldsymbol{\alpha}(\omega)$ is obtained in TWA, when the sample has a suitable finite thickness d. The complex heat capacity $\boldsymbol{C}(\omega)$ can be measured by TMDSC and ac calorimetry [16], provided the sample's thickness can be considered as negligibly small, i.e. the heat-transfer through the sample is relatively fast with respect to the temperature-modulation period.

On the other hand, the thermal parameters $\boldsymbol{\lambda}$ and $\boldsymbol{c}$ of a sample with a suitable finite thickness can be determined simultaneously from the measured two values T_0 and φ, provided the sample's thermal properties are frequency independent and not complex, i.e. in the temperature range far from a phase transition. Such measurements were made by a photopyroelectric technique [17–20], transient hot-strip method [21], thermal wave transmission spectroscopy [9,10,22,23], thermal wave analysis [8,24,25], and a laser flash technique [26–28].

The measurement of the temperature oscillations on both sides of a sample provides the *complete information* on both complex parameters $\boldsymbol{e}(\omega)$ and $\boldsymbol{\alpha}(\omega)$, as well as on complex $\boldsymbol{c}(\omega)$ and $\boldsymbol{\lambda}(\omega)$. The parameters $\boldsymbol{e}(\omega)$ and $\boldsymbol{\alpha}(\omega)$ can be obtained from two different measurements [19,29] or measured *simultaneously in the same experiment* [30,31]. As the investigated process can be reproduced only with some error, the possibility of simultaneous measurements of $\boldsymbol{e}(\omega)$ and $\boldsymbol{\alpha}(\omega)$ in *the same experiment* is preferable.

Recently, we reported on simultaneous measurements of the both complex thermal parameters $\boldsymbol{c}(\omega)$ and $\boldsymbol{\lambda}(\omega)$ near the glass transition in glycerol [31]. The temperature oscillations $T_{01} \sin(\omega t + \varphi_1)$ and $T_{02} \sin(\omega t + \varphi_2)$ on both sides of a plate-like sample were measured in a two-channel ac calorimeter. The amplitudes T_{01} and T_{02}, as well as the phases φ_1 and φ_2, contain the complete information on the sample's complex thermal parameters.

The aim of the present work is to further advance the two-channel ac calorimeter. In the new construction the sample is placed between two semi-infinite rods with metal-film heaters and temperature sensors sputtered on the faces of these rods, which are in direct thermal contact with the sample. In this construction, only two interfaces with thermal-wave reflections exist. In the previous construction, in which two sapphire substrates for support of the film heater and sensors were used, the number of the boundaries was as large as four plus the boundary between the holder and the ambient gas [31]. Such construction was very complicated and had too many unknown parameters, which have to be determined. The new measuring cell can be easily calibrated with higher precision and is simpler in handling. This improvement increased the accuracy of the measured sample's parameters.

Additional information can be obtained, besides the properties of the sample, in the region apart from phase transitions, where the sample's thermal

properties are not complex. Thus, the two-channel ac calorimeter provides the unique possibility of simultaneous measurements of the thermal contact properties together with the sample's thermal parameters. A stepwise change of the temperature-modulation amplitude at the cell/sample interface was observed and the value of this step was measured. The value of this step was extrapolated into the glass transition region and it was taken into account for the measurements of thermal properties of glycerol.

The capabilities of this advanced technique are demonstrated, being applied for simultaneous measurements of complex thermal parameters $\boldsymbol{e}(\omega)$ and $\boldsymbol{\alpha}(\omega)$, as well as $\boldsymbol{c}(\omega)$ and $\boldsymbol{\lambda}(\omega)$, in the glass transition region. In addition, the thermal conductivity, measured in the steady-state mode, can be detected in the same measuring cell. We present experimental data obtained for the glass transition in glycerol, which was used as a test material in other temperature-modulated [2,3,15,31–33], hot-wire [33,34], and standard steady-state [35] techniques.

2. The method: general description

Consider the following cylindrical system: a disk-shaped sample placed between two identical semi-infinite dielectric rods, as shown in Fig. 1. A metal-film heater and temperature sensors are sputtered on the polished ends of the rods, which are in direct thermal contact with the sample. The heat capacities and thermal resistances of the film heater and of the sensors are negligibly small. Thus, the system can be described by the following parameters: the thermal effusivity of the rods e_0, the cross-sectional area of the system S, and the sample's parameters: thickness d, complex thermal effusivity $\boldsymbol{e}(\omega)$ and complex thermal diffusivity $\boldsymbol{\alpha}(\omega)$.

The resistive film heater provide a uniform heat flow with an oscillating part $\mathrm{Re}[P_0 \exp(\mathrm{i}\omega t)]$, where the temperature-modulation frequency $f = \omega/2\pi$ equals the double frequency of the sinusoidal electric current. Denote the heat flux from the heater $\boldsymbol{q}(t) = q_0 \exp(\mathrm{i}\omega t)$, where $q_0 = P_0/S$. This heat flux is supplied to the first rod/sample interface at $x = 0$ and propagates through the system in both directions along the x-axis. We assume that the thermal oscillations are small enough to consider the linear-response approximation. Then, the stationary oscillating solution of the Fourier heat-transfer equation for this system is as follows. The running waves $\boldsymbol{T}_1(t, x) = \boldsymbol{T}_{01} \exp(\mathrm{i}\omega t + \boldsymbol{k}_0 x)$ and $\boldsymbol{T}_2(t, x) = \boldsymbol{T}_{02} \exp[\mathrm{i}\omega t - \boldsymbol{k}_0 (x - d)]$ are exited in the first and in the second semi-infinite rods, where $\boldsymbol{k}_0^2 = \mathrm{i}\omega c_0/\lambda_0$; c_0 is the specific heat capacity and λ_0 is the thermal conductivity of the rods. The standing wave $\boldsymbol{T}(t, x) = \exp(\mathrm{i}\omega t)[\boldsymbol{A} \sinh(\boldsymbol{k}x) + \boldsymbol{B} \cosh(\boldsymbol{k}x)]$ is exited in the sample, where $\boldsymbol{k}^2 = \mathrm{i}\omega \boldsymbol{c}/\boldsymbol{\lambda}$, with $\boldsymbol{c}$—complex specific heat capacity and $\boldsymbol{\lambda}$—complex thermal conductivity of the sample. The complex parameters $\boldsymbol{A}$, $\boldsymbol{B}$, $\boldsymbol{T}_{01}$, and

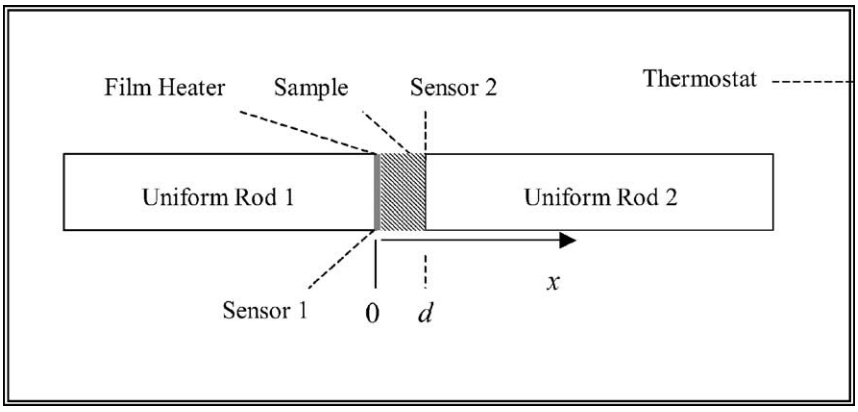

Fig. 1. Scheme of the experiment. The sample is placed between two identical semi-infinite dielectric rods. The metal-film heater and the first sensor are sputtered on the polished end of the first rod. The second sensor is sputtered on the second rod. The cell is placed into a thermostat.

$\boldsymbol{T}_{02}$ are determined by the boundary conditions for the heat flux and the temperature on both interfaces.

To describe our experimental results we had to take into account a discontinuity of the temperature oscillations at the cell/sample interface. Suppose that a thermal contact resistance—existing on an interface a/b between a medium "a" and a medium "b"—leads to a jump in the amplitude of the temperature oscillations. Thus, the boundary condition for the amplitudes of the temperature oscillations in medium "a" and "b" is as follows: $\eta \boldsymbol{T}_a = \boldsymbol{T}_b$, where η is a dimensionless parameter ca. 1, characterizing a stepwise change of the temperature-modulation amplitude on the interface. No change in the phase of the temperature oscillations on the interface is assumed, i.e. η is a real valued parameter. This assumption is in agreement with the experiment as shown below. Next, the heat flux is considered to be continuous as the energy is conserved.

Then, the complex amplitudes $\boldsymbol{T}_{01}$ and $\boldsymbol{T}_{02}$, which are measured on both sides of the sample, can be calculated as follows:

$$\boldsymbol{T}_{01} = q_0 \frac{[1 + \eta(e_0/\boldsymbol{e}) \tanh(d\boldsymbol{k})]}{\boldsymbol{F}}, \quad (1)$$

$$\boldsymbol{T}_{02} = \frac{\eta^2 q_0}{[\boldsymbol{F} \cosh(d\boldsymbol{k})]}, \quad (2)$$

where $\boldsymbol{F}(\omega) = (\mathrm{i}\omega)^{1/2}\ [(1 + \eta^2)e_0 + \eta(\boldsymbol{e} + e_0^2/\boldsymbol{e}) \tanh(d\boldsymbol{k})]$. Note, that $\boldsymbol{k}^2 = \mathrm{i}\omega/\boldsymbol{\alpha}$. Thus, the complex parameters $\boldsymbol{e}$ and $\boldsymbol{\alpha}$, as well as $\boldsymbol{c} = \boldsymbol{e}/(\boldsymbol{\alpha})^{1/2}$ and $\boldsymbol{\lambda} = \boldsymbol{e}(\boldsymbol{\alpha})^{1/2}$, can be obtained from the measured q_0 and complex amplitudes $\boldsymbol{T}_{01}$ and $\boldsymbol{T}_{02}$, provided the parameters e_0 and η were determined in advance. The calibration procedure is described below.

3. Measuring cell

The calorimeter was constructed for the frequency range 0.01–100 Hz. The measuring cell of the calorimeter is shown schematically in Fig. 1. The following two cells were fabricated. The first was made of machineable glass ceramic (MACOR^{TM} [36]) and the second of polyetheretherketone (PEEK) [37]. These materials have the following thermal parameters at room temperature: specific heat capacity ca. $2 \times 10^6\ \mathrm{J\,K^{-1}\,m^{-3}}$ [36] and $1.5 \times 10^6\ \mathrm{J\,K^{-1}\,m^{-3}}$ [37], and thermal conductivity ca. 1.5 and $0.25\ \mathrm{W\,K^{-1}\,m^{-1}}$ [36], respectively. Then, at frequencies higher 10 mHz a rod of length $L = 1$ cm can be considered as semi-infinite within accuracy ca. $|1 - \tanh(L\boldsymbol{k}_0)|$, which equals 2 and 0.03% for MACOR and PEEK, respectively. The rods in the cells were ca. 1 cm long and ca. 4.5 mm in diameter.

Consider the first cell, which consists of two identical rods made of MACOR. The copper–constantan thermocouples were sputtered on the polished ends of both rods. The thickness of constantan and copper films was ca. 100 nm. The copper–constantan intersection area—the sensing area—was ca. 3 mm × 3 mm and was placed in the center. Of course, the composition of the Ni–Cu alloy in the film sensors was not exactly the same as in the constantan target used for the film sputtering. Thus, the emf of the received thermocouples was ca. two times smaller than that of a standard copper–constantan thermocouple. Therefore, thermocouple calibration was required. These film sensors were covered by dielectric layers of ca. 1500 nm Al_2O_3. The nickel-film heaters of thickness ca. 30 nm were sputtered on these dielectric layers of both rods, so that the total area of the faces of the rods was covered by the heater-films. The resistance of the heaters was ca. 50 Ω.

It should be noted, that there were two sensors and two heaters on both sides of the cell. So, we have the possibility to use the second heater in addition to the first one. The additional heater can be used for a compensation of the temperature gradient in the sample, as well as for driving the sample temperature according to any program. For example, it may be a fast step heating. On the other hand, these nickel-films can be used for one-side or for double-side 3-ω measurements. In the present work, only one, the first heater, was utilized.

The cell made of polyetheretherketone has other sensors. These sensors were fabricated of copper and constantan wires of 50 μm diameter. The wires were welded together and flattened out to the thickness of 20–30 μm. Next, the flattened out thermocouples were fused into the surfaces of the PEEK rods. Then the ends of the rods were polished, so that the flat and polished thermocouples of 10–20 μm thickness were placed just on the flat surfaces of the rods. The emf of these sensors was exactly the same as of a standard copper–constantan thermocouple. Then, the

polished ends of the rods with these sensors were covered by dielectric layers of ca. 1500 nm Al_2O_3. Next, the nickel-film heaters, the same as in the first cell, were sputtered on the ends of the rods.

The empty cell calibration was performed at different temperatures and in the frequency range 0.01–100 Hz. A thin layer ca. 5 μm of Apiezon™-H grease was used as a surfactant for good thermal contact between the two identical parts of the cell. The heat-transfer through the thermocouple wires may effect the measured temperature oscillations. The heat-transfer is negligibly small in the case of the film thermocouple. The MACOR/MACOR cell with the film thermocouples was used to check the losses of the PEEK/PEEK cell with the wire thermocouples. The frequency dependencies of the amplitudes T_{01} and T_{02} and the phases φ_1 and φ_2 of both empty cells were similar in the whole frequency range 0.01–100 Hz. Therefore, the heat-transfer through the thermocouple wires was also negligibly small.

Although, the both PEEK and MACOR cells provide qualitatively the same results in the applied frequency and temperature ranges, nevertheless, the MACOR cell is better at temperatures above ca. 400 K. Unfortunately, the PEEK cell cannot be used at high temperatures, because of cracking of the Al_2O_3 dielectric film at heating due to the relatively high thermal expansion of PEEK, which is 10 times large than that of the dielectric film. The MACOR cell with the film thermocouples is also better for high frequency measurements, than the PEEK cell with the wire thermocouples. The only problem is the necessity of precise calibration of the film thermocouples. Thus, the development of the MACOR cells is still in progress. In this work, the MACOR cell was utilized only for verification of the frequency dependences. The results presented in this paper were obtained with the PEEK cell.

The temperature dependency of PEEK thermal effusivity $e_0(T)$ obtained from the empty-cell measurements was used as calibration data of this cell. The measured values were in agreement with the known data. For example, at room temperature the thermal conductivity of PEEK is equal to $0.25\,W\,K^{-1}\,m^{-1}$ [36] and the specific heat capacity equals 320–326 $J\,K^{-1}\,mol^{-1}$ [37], i.e. the effusivity $e_0 = 600 \pm 10\,J\,m^{-2}\,K^{-1}\,s^{-1/2}$ at density $\rho_0 = 1.29 \pm 0.03\,g\,cm^{-3}$ [36] and molecular weight $M = 288$ Da. The measured effusivity was $620 \pm 10\,J\,m^{-2}\,K^{-1}\,s^{-1/2}$ at 300 K. The same measurements for the other cell were also in agreements with the known data for MACOR. Thus, at room temperature λ_0 equals $1.5\,W\,K^{-1}\,m^{-1}$, $c_0 = 0.79\,J\,g^{-1}\,K^{-1}$ and $\rho_0 = 2.52\,g\,cm^{-3}$ [36], that is $e_0 = 1730\,J\,m^{-2}\,K^{-1}\,s^{-1/2}$ compared to the effusivity $1700 \pm 50\,J\,m^{-2}\,K^{-1}\,s^{-1/2}$ measured at 300 K. The calibration was independent on the ambient gas pressure in the range 0.1 to 10^3 mbar.

4. Interface jump of temperature-modulation amplitude

Once the cell calibration was performed, the complete set of the sample's thermal parameters can be determined from the measured complex amplitudes $\boldsymbol{T}_{01}$ and $\boldsymbol{T}_{02}$. Actually, the amplitudes $\boldsymbol{T}_{01}$ and the phase shifts $\varphi_i = \mathrm{Arg}(T_{0i})$ between the heat flux, $\boldsymbol{q}(t)$, and the temperature oscillations in the ith sensor are measured by a digital lock-in amplifier. Two lock-in amplifiers, EG&G Instruments 7265, were used for simultaneous measurements of the complex amplitudes $\boldsymbol{T}_{01}$ and $\boldsymbol{T}_{02}$ in the frequency range 0.01–100 Hz. For precise phase measurements, the internal generator of one of the lock-in amplifiers was used as the power source for the resistive heater. The following four parameters $\mathrm{Re}[\boldsymbol{e}(f)]$, $\mathrm{Im}[\boldsymbol{e}(f)]$, $\mathrm{Re}[\boldsymbol{\alpha}(f)]$, and $\mathrm{Im}[\boldsymbol{\alpha}(f)]$ were calculated according to Eqs. (1) and (2) from the amplitudes T_{01}, T_{02} and the phase shifts φ_1, φ_2 measured at a fixed frequency $f = \omega/2\pi$.

On the other hand, when the temperature is not close to a phase transition, the sample's thermal properties are not frequency-dependent and not complex. In this case, the four measured values T_{01}, T_{02}, φ_1 and φ_2 are determined by the only two *frequency independent* sample's parameters $e(T)$ and $\alpha(T)$ at any frequency. In this case, besides the properties of the sample additional information can be obtained. Thus, the stepwise change of the temperature-modulation amplitude on the cell/sample interface can be measured. The relative jump in the temperature-modulation amplitude at the interface can be described by a dimensionless parameter η, which characterizes the imperfection of the interface thermal contact. It is notorious that a thermal contact resistance is observed in the case of a dry thermal contact [38,39], as well as on a liquid/solid interface [40].

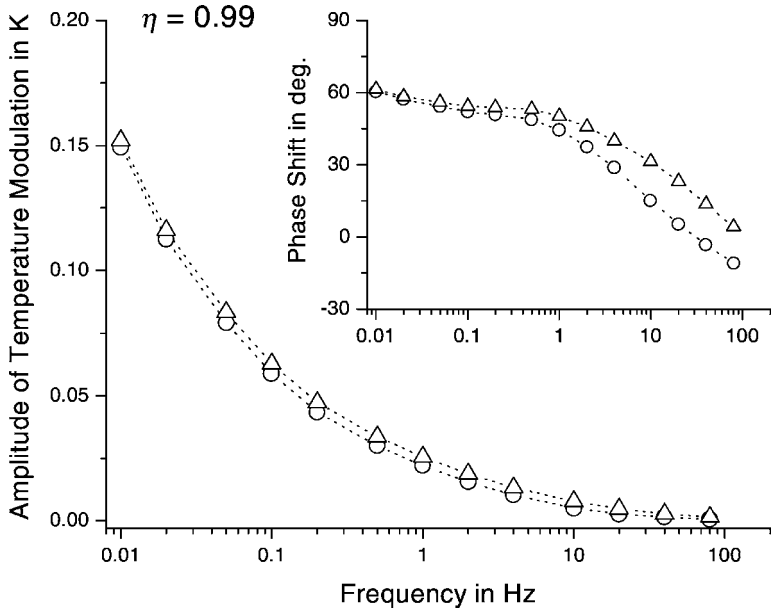

Fig. 2. Frequency dependencies of temperature-modulation amplitudes, T_{01} (triangles) and T_{02} (circles), and corresponding phase shifts on both thermal sensors for PEEK empty cell at 220 K and heat-flow amplitude 0.9 mW. The grease Apiezon^{TM}-H was used for a good thermal contact. The parameter η characterizing the interface jump in the temperature-modulation amplitude equals ca. 0.99.

The frequency dependences of the temperature-modulation amplitudes and of the corresponding phase shifts on both thermal sensors of the PEEK empty cell at 220 K are shown in Fig. 2. A thin layer ca. 5 μm of Apiezon^{TM}-H grease was used as a surfactant for a good thermal contact. In the case of an ideal thermal contact, the temperature-modulation amplitudes, as well as the phase shifts, must be the same on both sides of a thin layer at sufficiently low frequencies. As shown in Fig. 2, a step in the temperature-modulation amplitude exists even at low frequencies, when the Apiezon-layer thickness, ca. 5 μm, can be considered as infinitely small and the phase shifts are the same on both sides of the layer. In fact, in Apiezon^{TM}-H, the thermal length $(2\lambda_A/\omega c_A)^{1/2}$, is as large as ca. 2 mm at frequency 0.01 Hz, where $\lambda_A = 0.2\,W\,K^{-1}\,m^{-1}$ and $c_A = 1.6 \times 10^6\,J\,m^{-3}$ [41]. In this case, an interface step of ca. 1% in the temperature-modulation amplitude was observed, i.e. parameter η was ca. 0.99. The parameter η characterizes the relative change of the temperature-modulation amplitude. Therefore, it must be independent on heat-flow amplitude, at least when the linear approximation is correct. No dependency of η on the heat-flow amplitude was observed in the range 0.5–10 mW. The parameter η was slightly linear dependent on temperature.

The stepwise change of the modulation amplitude is better defined in the case of the glycerol sample as shown in Fig. 3. Similar results were observed with the MACOR cell. As both cells, PEEK and MACOR, were covered with the same films, the thermal contacts with the samples were the same. For both cells the thermal resistance of the film/cell interface was negligibly small. In case of a dry thermal contact at the cell/sample interface the step in the temperature-modulation amplitude was more pronounced. It is noteworthy that a step as large as ca. 25% was observed at the interface between the MACOR cell and an ethylene-1-octene copolymer sample. Thus, we have to take into account the stepwise change of the temperature-modulation amplitude at the interfaces.

The origin of the thermal contact resistance can be attributed to the interface phonon scattering. The thermal contact conductance of the Apiezon^{TM}-H grease is better than that of glycerol, as the Apiezon^{TM}-H grease is a very good surfactant. The stronger the interface coupling between the adjacent substances, the better the thermal contact.

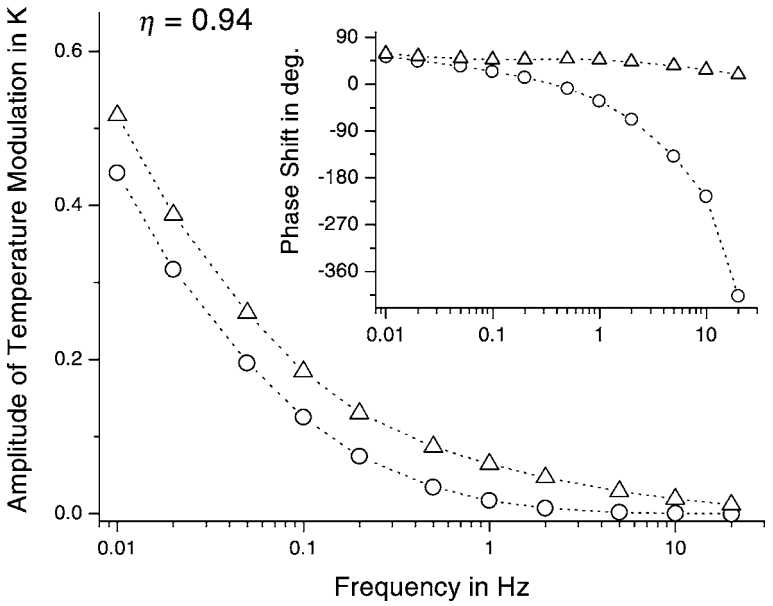

Fig. 3. Frequency dependences of temperature-modulation amplitudes, T_{01} (triangles) and T_{02} (circles), and corresponding phase shifts on both thermal sensors for the PEEK cell with a glycerol sample of 0.25 mm thickness at 220 K and heat-flow amplitude 3.1 mW. The parameter η equals ca. 0.94.

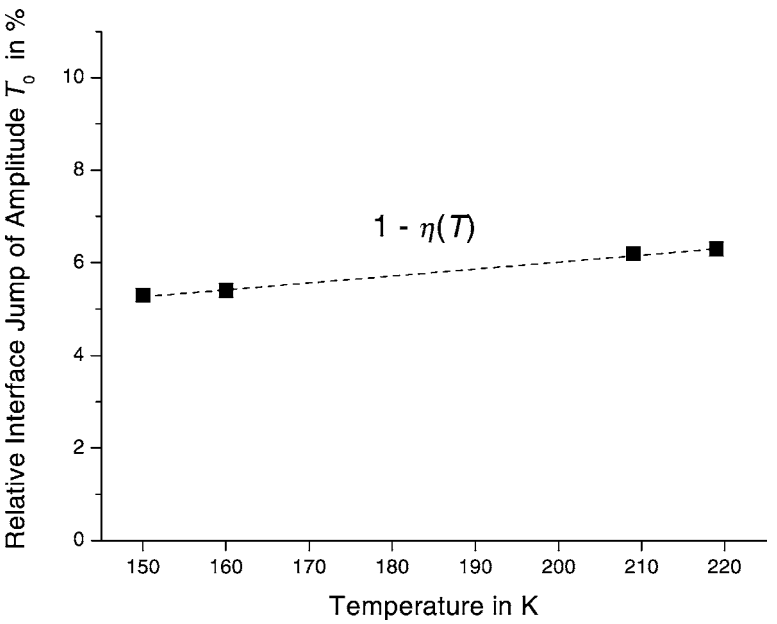

Fig. 4. Temperature dependence of the relative jump, $(1 - \eta)$ ca. 5%, in the amplitude of the temperature-modulation on the cell/glycerol interface at the same conditions as in Fig. 3.

In all these cases, the parameter η characterizing the interface jump in the modulation amplitude was slightly temperature dependent, so that the thermal contact was improved at cooling. The temperature dependence $\eta(T)$ was measured for the cell/glycerol interface above and below the glass transition region. Then, it was extrapolated into the glass transition region as shown in Fig. 4.

After calibration of the empty cell and determination of $\eta(T)$ for the cell/sample interface the sample's complex thermal properties can be measured in the glass transition region.

5. Experimental: results and discussion

The method was applied to study the glass transition in glycerol, $C_3H_8O_3$, which is a liquid with density ca. $1.26\,g\,cm^{-3}$ at room temperature and molecular weight $M = 92.1$ Da. Glycerol is a hygroscopic material and the samples always contain some amount of water. The glass transition studies in glycerol samples with 0.1 and 1% of H_2O yielded identical results [34]. The study of the glass transition in 75% (v/v) glycerol–water mixture showed that the qualitative behavior of the transition was the same in the mixture as in the pure glycerol [42], but the glass transition temperatures $T_g(f)$ were shifted to lower values with increasing water content. As we were interested in the qualitative features of the glass transition, we were not interested in glycerol samples of high purity. A 86/14 wt.% glycerol/water mixture, with the density $\rho = 1.23\,g\,cm^{-3}$, and a dried sample were investigated. The glycerol was received from Acros Organics Company.

Two samples of 0.25 and 0.6 mm thickness were investigated. A drop of calibrated volume $V = Sd$, where $S = 18.5\,mm^2$, was placed in the cell. The sample's thickness, 0.25 or 0.6 mm, was fixed by spacers. The temperature gradient across the sample can be estimated from the following relation: $\Delta T/d = P_0/2S\lambda$. The measurements were performed at the amplitude of the heat-flow rate $P_0 = 3.1$ mW, $S = 1.85 \times 10^{-5}\,m^2$ and $\boldsymbol{\lambda}$ ca. $0.3\,W\,K^{-1}\,m^{-1}$. Therefore, the temperature difference across the sample, ΔT, was equal to 0.07 and 0.17 K at $d = 0.25$ mm and 0.6 mm, respectively. Such temperature gradient in the sample was not essential.

The measurements were performed at a gas pressure of ca. 10 mbar. The heating–cooling cycling of the rate $1\,K\,min^{-1}$ was proceeded in the range 150–220 K. After the first heating–cooling cycle the results were reproducible and were the same at cooling and heating. The frequency dependences of the complex thermal parameters, $\boldsymbol{e}(f)$ and $\boldsymbol{\alpha}(f)$, were measured quasi isothermally at different temperatures in the range 150–220 K. Similar results for both samples were obtained. The sample of thickness 0.6 mm was investigated in the frequency range 0.01–6.0 Hz and the sample with $d = 0.25$ mm—in the range 0.02–10 Hz. The thermal properties of both samples were complex and frequency-dependent in the temperature region 170–200 K and in the frequency range 0.01–10 Hz as shown in Fig. 5. Such curves are typical for the relaxation process at glass transition. The extrema of the frequency dependencies $\mathrm{Im}[\boldsymbol{\alpha}(f)]$ and $\mathrm{Im}[\boldsymbol{e}(f)]$ correspond to the frequencies, at which $\mathrm{Re}(\boldsymbol{\alpha})$ and $\mathrm{Re}(\boldsymbol{e})$ are strongly frequency-dependent.

The temperature dependences of Re and Im parts of the frequency-dependent thermal diffusivity $\boldsymbol{\alpha}(f)$ at different frequencies for the sample of 0.25 mm thickness are shown in Fig. 6. The transition is shifted to higher temperatures at increasing frequency. The maxima of the dependencies $\mathrm{Im}[\boldsymbol{\alpha}(T)]$ approximately correspond to the middle of the step-like transition region of $\mathrm{Re}[\boldsymbol{\alpha}(T)]$. These temperature dependencies of $\mathrm{Re}(\boldsymbol{\alpha})$ and $\mathrm{Im}(\boldsymbol{\alpha})$ at different frequencies are typical for the relaxation process at a glass transition.

Frequency-dependent specific heat capacity $\boldsymbol{c}(f)$ and thermal conductivity $\boldsymbol{\lambda}(f)$ were obtained from the measured thermal diffusivity and effusivity according to the following relations: $\boldsymbol{c} = \boldsymbol{e}/(\boldsymbol{\alpha})^{1/2}$ and $\boldsymbol{\lambda} = \boldsymbol{e}(\boldsymbol{\alpha})^{1/2}$. The strong, ca. 50%, frequency dependence $\boldsymbol{c}(f)$ of the specific heat capacity was observed as shown in Fig. 7.

The complex heat capacity of a system is usually defined as $\boldsymbol{C}(\omega) = C'(\omega) - \mathrm{i}C''(\omega)$ [12–15], where the negative sign in the imaginary part of $\boldsymbol{C}(\omega)$ means the delay in the response of a system on the temperature-modulation $T(t) = T_0 \exp(\mathrm{i}\omega t)$. Of course, according to the principle of causality $C''(\omega)$ is positive [13], i.e. $\boldsymbol{C} = C\exp(-\mathrm{i}\phi)$ with positive ϕ and the response on the temperature-modulation equals $\boldsymbol{C}\,\mathrm{d}\boldsymbol{T}(t)/\mathrm{d}t = \mathrm{i}\omega C T_0 \exp[\mathrm{i}(\omega t - \phi)]$ with the positive delay ϕ. On the other hand, the response of the system on the temperature-modulation $T_0 \exp(-\mathrm{i}\omega t)$

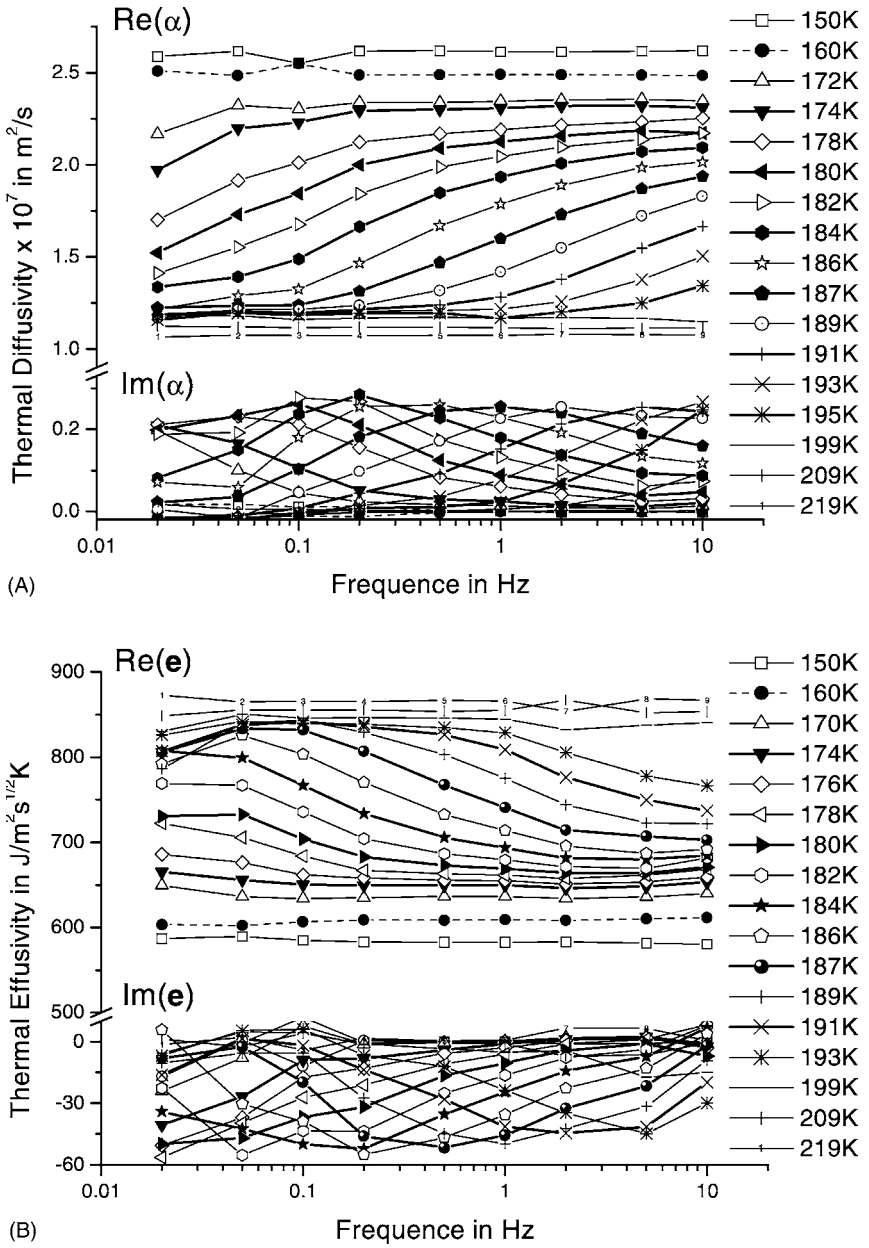

Fig. 5. Frequency dependences of Re and Im parts of (A) complex thermal diffusivity $\boldsymbol{\alpha}(f)$ and (B) complex thermal effusivity $\boldsymbol{e}(f)$ at different temperatures in the glass transition region for the sample of 0.25 mm thickness. The different signs of the imaginary parts are explained in the text. The experiment was performed at the heat-flow amplitude 3.1 mW.

is delayed when $\boldsymbol{C} = C\exp(\mathrm{i}\phi)$ at positive ϕ, i.e. $\boldsymbol{C}(\omega) = C'(\omega) + \mathrm{i}C''(\omega)$ and $C''(\omega) > 0$. The physical meaning of $C''(\omega)$ is as follows. Consider a system, which undergoes a temperature cycling. Assume, that the system is returned to it's initial state after each cycle. Then, owing to the delay of the system response the thermostat entropy is increased after each cycle, even if the system is returned to it's initial

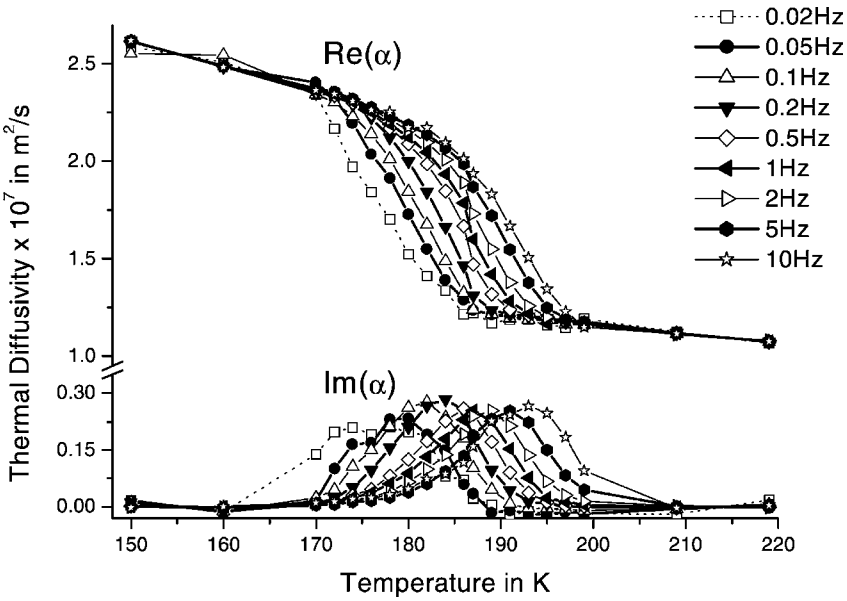

Fig. 6. Temperature dependences of Re and Im parts of the frequency-dependent thermal diffusivity $\boldsymbol{\alpha}(f, T)$ at different frequencies in the glass transition region at the same conditions as in Fig. 5.

state. The entropy change of the thermostat, ΔS, after one temperature-modulation cycle is positive, in agreement with the second low of thermodynamics, and equals $\Delta S = \pi(T_0/T)^2 C''(\omega)$ [2], where T is the average temperature of the system. Of course, the same relation for the entropy change follows for the both definitions, $\boldsymbol{C}(\omega) = C'(\omega) - \mathrm{i}C''(\omega)$ at $T(t) = T_0 \exp(\mathrm{i}\omega t)$, as well as for $\boldsymbol{C}(\omega) = C'(\omega) + \mathrm{i}C''(\omega)$ at $T(t) = T_0 \exp(-\mathrm{i}\omega t)$, with positive $C''(\omega)$. In any case, $\boldsymbol{C}(\omega)$ equals $\mathrm{Re}(\boldsymbol{C}) + \mathrm{iIm}(\boldsymbol{C})$ by definition of a complex number. Then, for the usual definition, $\boldsymbol{C}(\omega) = C'(\omega) - \mathrm{i}C''(\omega)$ at $T(t) = T_0 \exp(\mathrm{i}\omega t)$, we have the following imaginary part $\mathrm{Im}(\boldsymbol{C}) = -C''(\omega)$. Note, that the imaginary part of the specific heat capacity shown in Fig. 7 is $\mathrm{Im}(\boldsymbol{c}) = -c''(f)$, where $\boldsymbol{c}(f)$ is defined as $\boldsymbol{c}(f) = c'(f) - \mathrm{i}c''(f)$. Because complex thermal effusivity $\boldsymbol{e}(f)$ and complex thermal diffusivity $\boldsymbol{\alpha}(f)$ depend different way on complex heat capacity $\boldsymbol{c}(f)$ the imaginary parts have different sign.

Well defined steps in $\mathrm{Re}[\boldsymbol{c}(T)]$ and extrema in $\mathrm{Im}[\boldsymbol{c}(T)]$ were observed at the glass transition. The extrema of the dependences $\mathrm{Im}[\boldsymbol{c}(T)]$ correspond to the middle of the step-like transition region of $\mathrm{Re}[\boldsymbol{c}(T)]$. The glass transition temperatures $T_g(f)$ can be determined as the temperatures corresponding to the extrema of $\mathrm{Im}[\boldsymbol{c}(T)]$ or of the derivative $\mathrm{dRe}[\boldsymbol{c}(T)]/\mathrm{d}T$. The dependences $\mathrm{Re}[\boldsymbol{c}(T)]$ are in agreement with the results of the heat capacity measurements presented in [43,44]. The values of the specific heat capacity below and above glass transition, $1.2 \pm 0.05\,\mathrm{J\,K^{-1}\,cm^{-3}}$ and $2.5 \pm 0.1\,\mathrm{J\,K^{-1}\,cm^{-3}}$, that is $0.98 \pm 0.05\,\mathrm{J\,g^{-1}\,K^{-1}}$ and $2.03 \pm 0.1\,\mathrm{J\,g^{-1}\,K^{-1}}$, were in good agreement with the values $0.85\,\mathrm{J\,g^{-1}\,K^{-1}}$ and $1.9\,\mathrm{J\,g^{-1}\,K^{-1}}$ presented in [43]. Note that the density of the sample was equal to $1.23\,\mathrm{g\,cm^{-3}}$ and it was a glycerol–water mixture with a water content ca. 14%. The specific heat capacity of the mixture was higher, than that of the pure glycerol. The absolute error, ca. 5%, of the specific heat capacity measurements was determined by the uncertainty of the sample's geometry. The step of the specific heat capacity at glass transition, ca. $1.05 \pm 0.05\,\mathrm{J\,g^{-1}\,K^{-1}}$, was also in agreement with the result of a DSC experiment, $1.02\,\mathrm{J\,g^{-1}\,K^{-1}}$, and of TMDSC measurements, $0.97\,\mathrm{J\,g^{-1}\,K^{-1}}$, presented in [44].

It is remarkable, that the thermal conductivity $\boldsymbol{\lambda}$ determined from the thermal diffusivity and effusivity was not complex and was frequency independent in spite of the *strong frequency dependency of the both* parameters $\boldsymbol{e}(f)$ and $\boldsymbol{\alpha}(f)$. As shown in Fig. 8 no noticeable Im part and no frequency dependency of

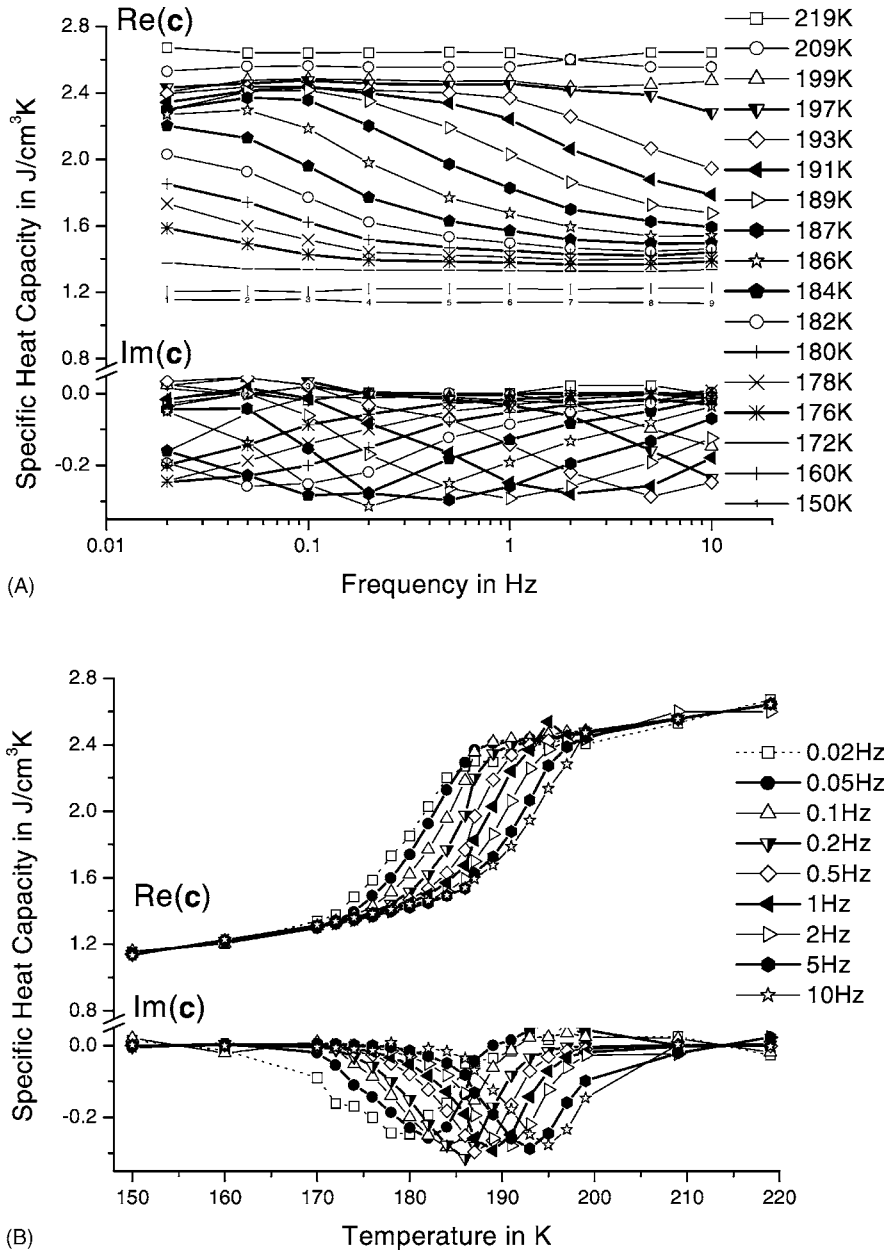

Fig. 7. Frequency (A) and temperature (B) dependences of Re and Im parts of the complex specific heat capacity $\boldsymbol{c}(f) = c'(f) - \mathrm{i}c''(f)$ in the glass transition region at the same conditions as in Fig. 5. Note, that the dependencies of $\mathrm{Im}(\boldsymbol{c}) = -c''(f, T)$ are plotted.

the thermal conductivity was observed in the curves $\mathrm{Re}[\boldsymbol{\lambda}(f)]$ and $\boldsymbol{\lambda}(T)$. At least the frequency dependence of the thermal conductivity was below the error of the experiment. It is noteworthy, that the error ca. 5% in the sample's geometrical parameters can lead only to a shift of the absolute values of $\boldsymbol{c}$ and $\boldsymbol{\lambda}$, calculated from the measured parameters $\boldsymbol{e}(f)$ and $\boldsymbol{\alpha}(f)$, without changing the frequency dependences. Therefore, the thermal conductivity of glycerol in the glass transition region can be considered as a real valued and frequency in-

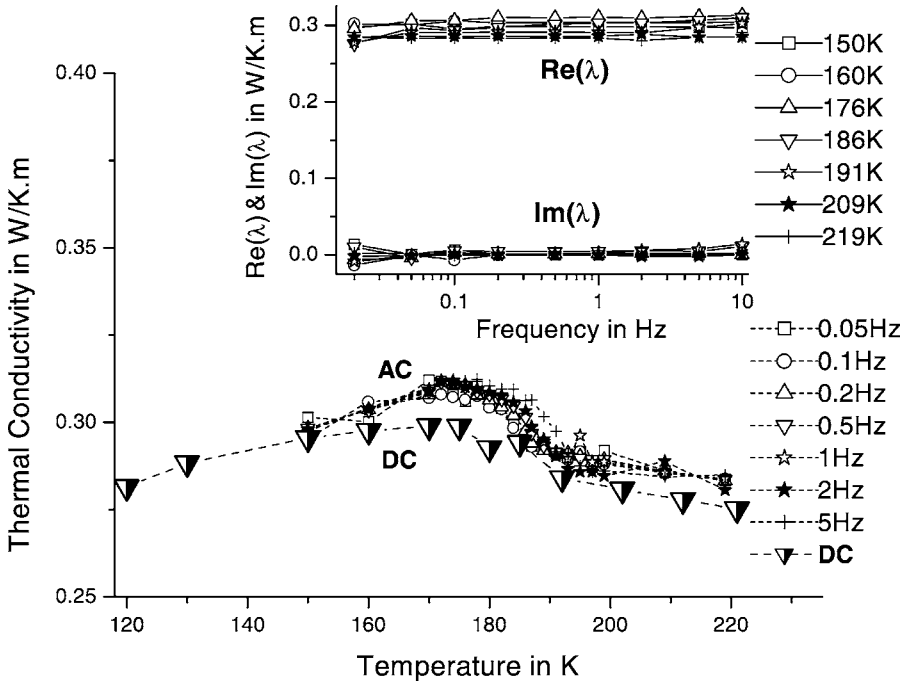

Fig. 8. Temperature dependences of the thermal conductivity absolute value $\boldsymbol{\lambda}$ measured at different frequencies, as well as in dc mode. The frequency dependencies of Re and Im parts of the thermal conductivity at different temperatures are shown in the insert. The ac measurements were performed at the same conditions as in Fig. 5. The dc experiment was carried out in the same cell at the heat flow rate 13 mW and the sample's thickness $d = 0.6$ mm.

dependent property in spite of the strong, ca. 50%, frequency dependence of the complex heat capacity. Of course, the thermal conductivity in amorphous material is not proportional to the specific heat capacity, as it is in crystals, because a phonon mean-free path would be as small as the inter-atomic distance and the phonon gas theory is not valid in this case. Thus, a change of the heat capacity not necessarily effects on the thermal conductivity in glasses.

Next, we consider the temperature dependence of the thermal conductivity absolute value $\boldsymbol{\lambda}$. An artificial peak in $\boldsymbol{\lambda}(T)$ can be observed in dynamic thermal conductivity measurements at T_g due to the frequency dependence of $\boldsymbol{c}(f)$. Such peak was observed for glycerol in [33,34]. On the other hand, as it was shown in [3,6], the apparent peak in $\boldsymbol{\lambda}(T)$ was due to nonzero Im part of $\boldsymbol{c}(f)$, which was neglected in the analysis of the experimental data for the thermal conductivity in [33,34]. This anomaly disappears, provided one takes into account the nonzero Im part of the heat capacity. As shown in Fig. 8 we did not find any anomaly and frequency dependence of the thermal conductivity in the glass transition region. The broad maximum, shown in Fig. 8, was not frequency-dependent and was observed in dc measurements too. The dc measurements of $\boldsymbol{\lambda}(T)$ were performed by a standard steady-state method in the same cell with the sample of 0.6 mm thickness at the constant heat flow rate of 13 mW. The temperature gradient across the sample was measured by the two sensors on both sides of the sample. The thermal contact resistance in the steady-state experiment was not determined. This is the reason why the thermal conductivity, measured in dc mode, was smaller than $\boldsymbol{\lambda}(T)$ measured in the ac experiment.

The broad maximum of $\boldsymbol{\lambda}(T)$ below the glass transition, shown in Fig. 8, was also observed in glycerol by other methods [33–35]. In general, the thermal conductivity must tend to zero at low temperatures. Therefore, as the thermal conductivity of glycerol increases with decreasing temperature above the glass

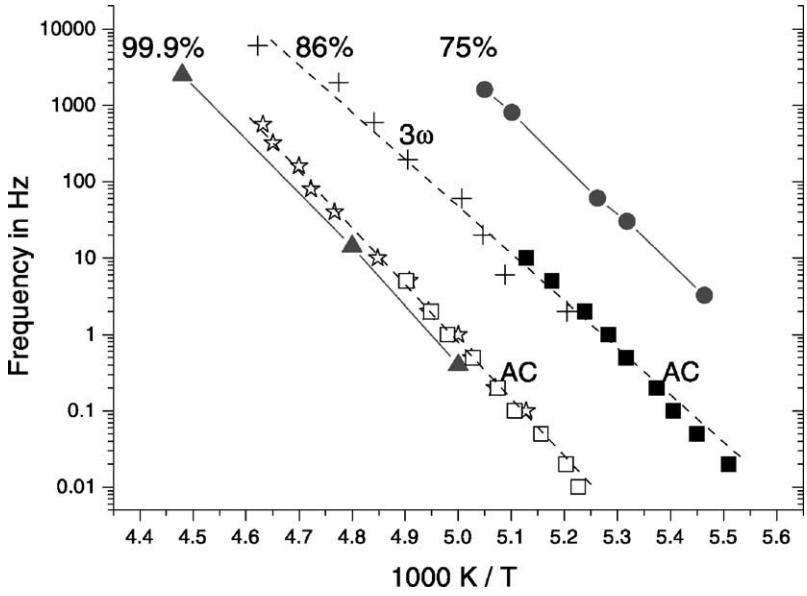

Fig. 9. Activation diagram of 86 wt.% glycerol–water mixture obtained by ac calorimetry (squares) and 3-ω method (crosses), as well as of dried glycerol obtained by ac calorimetry from heat capacity (open squares) and from thermal effusivity (stars). The results of Birge and Nagel [2] for pure glycerol (triangular) and of Settles et al. [42] for 75 vol.% glycerol–water mixture (circles) were received from 3-ω and dielectric spectroscopy techniques, respectively.

transition, $\boldsymbol{\lambda}(T)$ must have a maximum at temperatures below T_g.

As shown in Fig. 8 the thermal conductivity in the maximum equals ca. $0.31 \pm 0.02\,W\,K^{-1}\,m^{-1}$ and ca. $0.28 \pm 0.02\,W\,K^{-1}\,m^{-1}$ at 220 K. This result is in agreement with $\boldsymbol{\lambda}(T)$ ca. 0.32–0.30 $W\,K^{-1}\,m^{-1}$ measured in the same temperature range in [34].

The frequency dependence of the glass transition temperature $T_g(f)$ at low and intermediate frequencies was determined from the maxima of the derivative $d\mathrm{Re}[\boldsymbol{c}(T)]/dT$. The dependence $T_g(f)$ obtained by the two-channel ac calorimeter for the 86 wt.% glycerol–water mixture is shown in Fig. 9. The same sample was investigated by a 3-ω method at high frequencies. The points obtained by ac calorimetry are on the same line with the points received from the 3-ω measurements. Next, the activation diagram was measured for glycerol dried at 120 °C at 0.1 mbar during ca. 3 h. The water content was unknown in this sample, but the sample was close to pure glycerol. To illustrate the capability of the calorimeter we determined the high frequency part of the diagram from the maxima of the derivative $d\mathrm{Re}[\boldsymbol{e}(T)]/dT$, when the sample can be considered as semi infinite and the effusivity was determined from the only signal on the first side. The absolute calibration was not necessary for these relative measurements. Thus, the activation diagram was determined in the relatively broad frequency range 0.01–560 Hz. The dependence $T_g(f)$ is in agreement with the results from the heat capacity spectroscopy [2,3,15,32] and dielectric spectroscopy [45–48] of glycerol and dielectric spectroscopy of 75% (v/v) glycerol–water mixture [42]. The curve $1/T_g(f)$ is shifted to the lower temperatures at increasing water contamination as shown in Fig. 9.

6. Conclusions

The advanced two-channel ac calorimetry can be applied for simultaneous measurements of the complete set of the frequency-dependent complex thermal parameters at phase transitions in the same experiment. This is a method for simultaneous and *direct*

measurements of the complex thermal effusivity and diffusivity, as well as of the specific heat capacity and thermal conductivity. This technique can be applied for different materials, when the complex amplitudes of the temperature-modulations can be measured on both sides of the sample. The method provides a possibility to answer the fundamental question about the value of Im part of the thermal conductivity at phase transitions. It was found, that the thermal conductivity of glycerol in the glass transition region is a real valued and frequency independent property in spite of the strong, ca. 50%, frequency dependence of the complex heat capacity.

It is remarkable, that the thermal conductivity λ was frequency independent in spite of the *strong frequency dependency* of the parameters $e(f)$ and $\alpha(f)$, from which λ was determined. This means that the double-channel ac calorimetry is a technique, which can be used for reliable distinguishing of relaxation processes related to relaxing thermal conductivity or relaxing heat capacity.

On the other hand, in the region apart from a phase transition the double-channel calorimeter provides the unique possibility of simultaneous measurements of the thermal contact properties together with the sample's thermal parameters. The discontinuity of the temperature oscillations at the cell/sample interface was observed and the parameter characterizing this discontinuity was measured. The improvement of the accuracy gave us the possibility to measure the step in the temperature-modulation amplitude of ca. 1% even in the case of a good thermal contact formed by the surfactant Apiezon^{TM}-H grease. In case of a dry thermal contact at the cell/sample interface the step in the temperature-modulation amplitude can be more pronounced. A step as large as ca. 25% was observed at the interface between the MACOR cell and an ethylene–1-octene copolymer sample. Thus, the thermal contact resistance must be taken into account in temperature-modulated calorimetry, especially in the case of a dry cell/sample contact.

Acknowledgements

The financial support of the German Science Foundation (DFG), grant numbers SCHI 331/7 and 436 RUS 17/108/01 is gratefully acknowledged.

References

[1] H. Gobrecht, K. Hamann, G. Willers, J. Phys. E: Sci. Instrum. 4 (1971) 21.
[2] N.O. Birge, S.R. Nagel, Phys. Rev. Lett. 54 (1985) 2674.
[3] N.O. Birge, Phys. Rev. B 34 (1986) 1631.
[4] B. Buchner, P. Korpiun, Appl. Phys. B 43 (1987) 29.
[5] I.K. Moon, Y.H. Jeong, S.I. Kwun, Rev. Sci. Instrum. 67 (1996) 29.
[6] Y.H. Jeong, Thermochim. Acta 304–305 (1997) 67.
[7] T. Hashimoto, J. Morikawa, T. Kurihara, T. Tsuji, Thermochim. Acta 304–305 (1997) 151.
[8] J. Morikawa, T. Hashimoto, Thermochim. Acta 352 (2000) 291.
[9] A.A. Minakov, Yu.V. Bugoslavsky, C. Schick, Thermochim. Acta 317 (1998) 117.
[10] A.A. Minakov, Yu.V. Bugoslavsky, C. Schick, Thermochim. Acta 342 (1999) 7.
[11] A.A. Minakov, Thermochim. Acta 304–305 (1997) 165.
[12] J.E.K. Schawe, Thermochim. Acta 260 (1995) 1.
[13] J.E.K. Schawe, Thermochim. Acta 271 (1996) 127.
[14] J.E.K. Schawe, G.W.H. Hohne, J. Therm. Anal. 46 (1996) 893.
[15] C. Schick, G.W.H. Hohne, Temperature modulated calorimetry, Thermochim. Acta 304–305 (1997) (special issue).
[16] R. Nozaki, H. Nakano, N. Noda, H. Haga, Y. Shiozaki, J. Korean Phys. Soc. 29 (1996) S736.
[17] U. Zammit, M. Marinelli, R. Pizzoferrato, F. scudieri, S. martellucci, J. Phys. E: Sci. Instrum. 21 (1988) 935.
[18] M. Marinelli, F. Mercuri, S. Foglietta, D.P. Belanger, Phys. Rev. B 54 (1996) 4087.
[19] J. Thoen, C. Glorieux, Thermochim. Acta 305 (1997) 137.
[20] J. Caerels, C. Glorieux, J. Thoen, Rev. Sci. Instrum. 71 (2000) 3506.
[21] Y.W. Song, U. Gross, E. Hahne, Fluid Phase Equilib. 88 (1993) 291.
[22] A.A. Minakov, C. Schick, Thermochim. Acta 330 (1999) 109.
[23] A.A. Minakov, Thermochim. Acta 345 (2000) 3.
[24] J. Morikawa, T. Hashimoto, A. Maesono, High Temperatures-High Pressures 33 (2001) 387.
[25] J. Morikawa, T. Hashimoto, J. Therm. Anal. Calorim. 64 (2001) 403.
[26] C. Ronchi, M. Sheindlin, M. Musella, G.J. Hyland, J. Appl. Phys. 85 (1999) 776.
[27] K. Shinzato, T. Baba, J. Therm. Anal. Calorim. 64 (2001) 413.
[28] J. Sun, J.P. Longtin, T.F. Irvine, Int. J. Heat Mass Transfer 44 (2001) 645.
[29] T. Albrecht, S. Armbruster, B. Stuhn, K. Vogel, G. Strobl, Thermochim. Acta 377 (2001) 159.
[30] Yu.I. Polikarpov, A.I. Slutsker, Thermochim. Acta 304–305 (1997) 277.
[31] A.A. Minakov, S.A. Adamovsky, C. Schick, Thermochim. Acta 377 (2001) 173.
[32] N.O. Birge, P.K. Dixon, N. Menon, Thermochim. Acta 304–305 (1997) 51.

[33] D.G. Cahill, R.O. Pohl, Phys. Rev. B 35 (1987) 4067.
[34] O. Sandberg, P. Andersson, G. Backstrom, J. Phys. E: Sci. Instrum. 10 (1977) 474.
[35] C. Talon, Q.W. Zou, M.A. Ramos, R. Villar, S. Vieira, Phys. Rev. B 65 (2001) 1.
[36] Technical data available on the website: http://www.goodfellow.com/.
[37] Athas databank: http://web.utk.edu/~athas/.
[38] J.J. Fuller, E.E. Marotta, J. Therm. Phys. Heat Transfer 15 (2001) 228.
[39] E. Marotta, L.S. Fletcher, T. Aikawa, K. Maki, Y. Aoki, J. Heat Transfer 121 (1999) 177.
[40] J.S. Olafsen, R.P. Behringer, J. Low Temp. Phys. 106 (1997) 673.
[41] Technical data available on the website: http://www.apiezon.com/.
[42] M. Settles, F. Post, D. Muller, A. Schulte, W. Doster, Biophys. Chem. 43 (1992) 107.
[43] P. Claudy, J.C. Commercon, J.M. Letoffe, Thermochim. Acta 128 (1988) 251.
[44] E. Hempel, G. Hempel, A. Hensel, C. Schick, E. Donth, J. Phys. Chem. B 104 (2000) 2460.
[45] K.L. Ngai, R.W. Rendell, Phys. Rev. B 41 (1989) 754.
[46] C. Hansen, R. Richert, J. Phys.: Condens. Matter. 9 (1997) 9661.
[47] N. Menon, K.P. O'Brien, P.K. Dixon, L. Wu, S.R. Nagel, J. Non-Cryst. Solids 141 (1992) 61.
[48] B. Schiener, B.V. Chamberlin, G. Diezemann, R. Bohmer, J. Chem. Phys. 107 (1997) 7746.